ORIGINAL ARTICLE

Microbial population and functional dynamics associated with surface potential and carbon metabolism

Shun'ichi Ishii[1,2,3,5], Shino Suzuki[1,5], Trina M Norden-Krichmar[1,6], Tony Phan[1], Greg Wanger[1], Kenneth H Nealson[1,4], Yuji Sekiguchi[2], Yuri A Gorby[1,4] and Orianna Bretschger[1]

[1]J. Craig Venter Institute, La Jolla, CA, USA; [2]Biomedical Research Institute, National Institute of Advanced Industrial Science and Technology (AIST), Tsukuba, Ibaraki, Japan; [3]Japan Society for the Promotion of Science (JSPS), Chiyoda-ku, Tokyo, Japan and [4]Department of Earth Sciences, University of Southern California, Los Angeles, CA, USA

Microbial extracellular electron transfer (EET) to solid surfaces is an important reaction for metal reduction occurring in various anoxic environments. However, it is challenging to accurately characterize EET-active microbial communities and each member's contribution to EET reactions because of changes in composition and concentrations of electron donors and solid-phase acceptors. Here, we used bioelectrochemical systems to systematically evaluate the synergistic effects of carbon source and surface redox potential on EET-active microbial community development, metabolic networks and overall electron transfer rates. The results indicate that faster biocatalytic rates were observed under electropositive electrode surface potential conditions, and under fatty acid-fed conditions. Temporal 16S rRNA-based microbial community analyses showed that *Geobacter* phylotypes were highly diverse and apparently dependent on surface potentials. The well-known electrogenic microbes affiliated with the *Geobacter metallireducens* clade were associated with lower surface potentials and less current generation, whereas *Geobacter* subsurface clades 1 and 2 were associated with higher surface potentials and greater current generation. An association was also observed between specific fermentative phylotypes and *Geobacter* phylotypes at specific surface potentials. When sugars were present, *Tolumonas* and *Aeromonas* phylotypes were preferentially associated with lower surface potentials, whereas *Lactococcus* phylotypes were found to be closely associated with *Geobacter* subsurface clades 1 and 2 phylotypes under higher surface potential conditions. Collectively, these results suggest that surface potentials provide a strong selective pressure, at the species and strain level, for both solid surface respirators and fermentative microbes throughout the EET-active community development.
The ISME Journal (2014) **8**, 963–978; doi:10.1038/ismej.2013.217; published online 19 December 2013
Subject Category: Microbial population and community ecology
Keywords: anode biofilm; microbial community dynamics; microbial fuel cell; per-biomass electrode reducing rate; 16S rRNA clone analysis

Introduction

Microbial extracellular electron transfer (EET) to solid surfaces is a key reaction for dissimilatory metal reduction in various anoxic environments and important to biogeochemical metal and nutrient cycling (Canfield *et al.*, 1993; Nealson, 1997; Nealson *et al.*, 2002; Weber *et al.*, 2006). In anoxic

Correspondence: S Ishii or S Suzuki, Microbial & Environmental Genomics, J. Craig Venter Institute, 4120 Torrey Pines Road, La Jolla, CA 92037, USA.
E-mail: sishii@jcvi.org or shishii@jcvi.org
[5]These authors contributed equally to this work.
[6]Present address: The Scripps Research Institute, La Jolla, CA 92037, USA.

environments, complex carbon substrates are degraded by fermenting microorganisms, and the by-products of the fermentation process, such as volatile fatty acids and hydrogen, are utilized as electron donors for subsequent microbial respiration of nitrate and sulfate, and the reduction of solid metals through microbial EET reactions (Nealson and Saffarini, 1994; Lovley *et al.*, 2004). The diversity and abundance of carbon sources in the environment is known to have a selective effect on microbial community taxonomy and function (Sessitsch *et al.*, 2001; Torsvik and Ovreas, 2002). Electron acceptors, including solid-phase electron acceptors, also have a selective role in determining microbial activity and population distributions (Humayoun *et al.*, 2003). In the environment, various forms of metal compounds exist and each

solid-phase compound has a different surface redox potential (Cornell and Schwertmann, 2003; Kato *et al.*, 2010), which could be having a significant role toward defining microbial population distributions. However, it is challenging to study the relationship between the surface redox potential and microbial population dynamics within the complex EET-active community, because the form and the redox potential of solid metals are changing that are associated with microbial metal-reducing functions.

Microbial fuel cells (MFCs) and poised-potential bioelectrochemical systems now offer a way to explore the relationship between microbial EET processes and solid surface potentials (Rabaey and Verstraete, 2005; Logan *et al.*, 2006; Lovley, 2006). The MFC anode electrode serves as an electron acceptor that can mimic solid metals, but does not react, and therefore serves as an unchanging solid-form electron acceptor. Using electrochemical approaches in MFC systems, the EET activity in a microbial community can be monitored as operational current generation, anodic limiting (maximum) current density and per-biomass electrode reducing rate throughout system operations (Ishii *et al.*, 2008). In addition, the anode potential can be controlled by potentiostatic set-potential (SP) operation (Wagner *et al.*, 2010), which allows acceleration or suppression of EET rates in the community as a function of applied surface redox potential (Aelterman *et al.*, 2008; Ishii *et al.*, 2013).

Recently, these methods have been utilized for exploring the microbial energy recovery with a wide variety of carbon substrates as electron donors (Pant *et al.*, 2010) and various controlled anode potentials as electron acceptors (Wagner *et al.*, 2010). These studies revealed that different EET-active communities were established with various carbon substrates and different electrode potentials, and both parameters clearly affected the final community composition (Torres *et al.*, 2009; White *et al.*, 2009; Freguia *et al.*, 2010; Kiely *et al.*, 2011). However, it is poorly understood how the substrates and electrode potentials affect the developmental processes of EET-active microbial communities, and how metabolic networks are established and maintained within the community. This knowledge is critical for expanding our understanding of community-wide EET processes with regard to microbe–microbe and microbe–environment interactions.

Therefore, objectives of this study were to identify the factors associated with EET-active (electrogenic) community development, and characterize the metabolic networks of the community members through the systematic integration of electrochemical and microbial analyses. To achieve the objectives, four different carbon substrates including two fermentable (sucrose and glucose) and two non-fermentable substrates (butyrate/propionate and acetate)

were employed as a variety of electron donors for developing EET-active microbial communities. In addition, three different electrode potentials with the sole fermentable substrate (sucrose) were also employed as a various electron acceptor's availability for the communities. Throughout the study, we constantly monitored electrochemical properties, biocatalytic activities, carbon metabolism and microbial community structure. A systematic integration and statistical analysis of the combined data sets offers new insights about the critical determining factors for EET-active microbial communities.

Materials and methods

MFC configuration and operation
Nine single-chamber, air-cathode MFCs were used for the enrichment of electrogenic communities fed with four different substrates. The MFC was a bottle-type reactor (400 ml in capacity), with anode electrodes made of carbon cloth ($108\,cm^2$ projected surface area; Tsukuba Materials Information Lab, Tsukuba, Japan) connected by Ti wires (Ishii *et al.*, 2008). A Pt-catalyzed air cathode as described elsewhere (Cheng *et al.*, 2006) was placed at the side port, providing a projected surface area of $20\,cm^2$. After sterilization of the MFC, the chamber was anaerobically filled with carbonate-buffered basal salt medium described in Supplementary Methods, which is modified from the previous research (Ishii *et al.*, 2008).

In an anaerobic glove box, 2 g of lagoon sediment slurry, sampled from San Elijo Lagoon (San Diego, CA, USA), was inoculated to the nine MFC reactors (Supplementary Figure S1). Four different carbon substrates (that is, 15 mM of acetate for AC-MFCs, mixture of 3.75 mM butyrate and 3.75 mM propionate for BP-MFCs, 5 mM of glucose for GL-MFCs or 2.5 mM of sucrose for SU-MFCs) were fed to duplicate MFC systems (reactors a and b). Within SU-MFCs, one reactor (reactor SU-MFC-a) did not begin electricity production, therefore one additional reactor (reactor SU-MFC-c) was started at day 22 with the same inoculum source stored at 4 °C. The MFCs were gently agitated with a magnetic stirrer and incubated at 28 °C.

Initially, the anode and cathode electrodes were connected with an external resistor of $510\,\Omega$. Cell voltages across the resistor were recorded every 10 min using a 2700 Multimeter data acquisition system with M7700 module (Keithley, Cleveland, OH, USA) and the corresponding electric current was calculated using Ohm's law. When the electric current decreased owing to the depletion of the substrates, the anode solutions were fully discarded and the reactors were refilled with fresh medium containing the appropriate substrate (the potential solution carry-over was estimated as $\sim1\%$ for each batch). This repeat-batch process was continued for
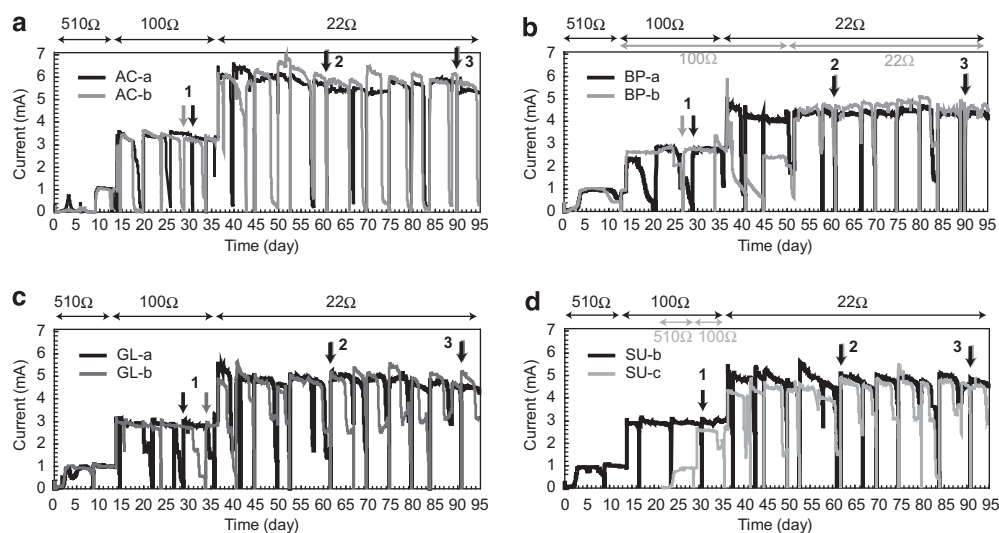
Figure 1 Electrical current generation in duplicate air-cathode MFCs fed with four different substrates. Duplicate MFCs (**a**, **b** or **c**) were operated with the external resistor described above the panels: (**a**) MFCs fed with acetate (AC-MFC); (**b**) MFCs fed with a mixture of butyrate and propionate (BP-MFC); (**c**) MFCs fed with glucose (GL-MFC); (**d**) MFCs fed with sucrose (SU-MFC). Arrows indicate anode biofilm sampling for DNA extraction and biomass determination.

over 3 months. The external resistor was changed twice to $100\,\Omega$ and $22\,\Omega$ as described in Figure 1.

SP operation
Six more reactors of the same configuration were used for SP operation fed with 3 mM sucrose as the sole electron donor. Before starting the SP operation, all reactors were operated on MFC mode for the first 5 days with a $510\,\Omega$ external resistor as described above. An Ag/AgCl reference electrode ($+200\,mV$ vs SHE, RE-5B, BASi, West Lafayette, IN, USA) was placed in the side port of duplicate SP reactors (reactors a or b), and the anode surface potential was controlled to $+100\,mV$ vs SHE (SP-H reactors), $-50\,mV$ vs SHE (SP-M reactors) and $-200\,mV$ vs SHE (SP-L reactors) using an eight-channel potentiostat (MultEchem System, Gamry, Warminster, PA, USA). The SP reactors were also anaerobically inoculated with 2 g of the same lagoon sediment stored at $4\,°C$, gently agitated at $28\,°C$ and electric current production was recorded every 10 min using the potentiostat. When the electric current decreased owing to the depletion of the substrates, the anode solutions were fully discarded and the reactors were refilled with fresh medium containing 3 mM sucrose. This repeat-batch process was continued for over 5 months.

Polarization analyses
In order to obtain anode polarization curves, an Ag/AgCl reference electrode (RE-5B, BASi) was placed in the side port of the reactors, and linear sweep voltammetry analyses were conducted using a potentiostat (Reference 600 or MultEchem System,

Gamry) (Tsujimura *et al.*, 2001; Ishii *et al.*, 2008). The anode potential was swept from open-circuit anode potential to $+300\,mV$ vs SHE at a scan rate of $0.5\,mV\,s^{-1}$ and the corresponding anodic current was recorded.

Chemical analyses
Volatile fatty acid concentrations were measured using a high-pressure liquid chromatography machine. The detailed procedures are described in Supplementary Methods. Glucose and sucrose concentrations were determined by the phenol-sulfuric acid method (Dubois *et al.*, 1979). Coulombic efficiency (%) was calculated from the total charge passed during a single batch, divided by the theoretical amount of charge allowable from complete substrate oxidization (for example, 48 mmol of e^- for AC-, GL- and SU-MFCs, 51 mmol of e^- for BP-MFC and 58 mmol of e^- for SP reactors in each batch) (Thauer *et al.*, 1977). To determine the total anodic microbial cell density, part of the anode ($7 \times 7\,mm$) was removed from the reactors ($n = 3$). Total protein was extracted and determined by the bicinchoninic acid method (Pierce, Rockford, IL, USA) as described elsewhere (Bond and Lovley, 2003; Ishii *et al.*, 2008).

Microbial composition analysis
Total DNA was extracted from biofilms on anodic carbon clothes or from suspended cells in anolyte solution using the PowerBiofilm DNA Isolation Kit (MO BIO, Carlsbad, CA, USA). The 16S rRNA clone libraries were constructed using universal primers U27f (5′-AGAGTTTGATCCTGGCTCAG-3′) and U1492r (5′-GGTTACCTTGTTACGACTT-3′) (DeLong, 1992), and

966

sequenced using primer U907r (5′-CCGYCAATT CMTTTRAGTTT-3′) (Watanabe et al., 2001) as described previously (Ishii et al., 2012). The nucleotide sequences have been deposited in the GSDB/ DDBJ/EMBL/NCBI nucleotide sequence databases under accession numbers JQ654784–JQ654964, JX145950–JX146061 and KC574687–KC574877. Database searches for related 16S rRNA gene sequences were conducted using the BLAST program (Karlin and Altschul, 1990). Identification of chimeric sequences, taxonomic classification and statistical analyses including multidimensional scale plot, rarefaction analysis, Chao-1 richness, Shannon's index, Simpson diversity index and Sørensen similarities among the bacterial communities were performed as described previously (Ishii et al., 2012). Canonical correspondence analysis (CCA) was performed using XLSTAT (Addinsoft, New York, NY, USA) to evaluate the correlations between community composition and environmental factors (ter Braak, 1986).

Results

MFC and SP enrichment and current generation
Duplicate MFC reactors (reactors a/c and b) fed with each carbon source showed similar current-generating trends during the 3-month operation in repeat-batch MFC mode (Figure 1). The medium replacement process removed suspended microbes and reduced the contribution of any redox-active soluble electron shuttles that may have been produced by the bacteria. To establish electrogenic communities, the external resistor was decreased stepwise from 510 Ω to 22 Ω (Figure 1), which has been successfully demonstrated to improve MFC electron recovery (Fan et al., 2008; Shimoyama et al., 2008; Hong et al., 2011; Jung and Regan, 2011). After day 50, all MFCs were producing stable operational currents of 5–7 mA. MFC performance metrics are summarized in Table 1.

Compared with the MFC operations, duplicate SP reactors (reactors a and b) fed with sucrose under three different anode potentials showed slightly different trends for the initial 50 days in the SP-H and SP-M reactors, and very different trends in the SP-L reactors (Figure 2). The SP-L-b reactor started generating current more slowly than the SP-L-a reactor, indicating that an anode potential of − 200 mV vs SHE may not have been a favorable selective pressure to reproducibly select for similar microbial EET activities. In contrast, the SP-H reactors showed a rapid startup of current generation within 10 days, and reached maximum operational current within 20 days. The maximum operational currents for each repeat-batch were ∼ 30 mA for SP-H, ∼ 20 mA for SP-M and 3–7 mA for SP-L, respectively. These differences are likely induced by the electron acceptor availability associated with the different anode potentials. The maximum operational current of the SP-H reactors decreased to ∼ 20 mA at 5 months, which suggests that biofilm features of the anodic community changed during the long-term SP-H operation. The electrogenic performances for the SP reactors are summarized in Table 2 for the 2-month (phase I) and 5-month (phase II) operational periods (Figure 2).

Limiting current density
Performance of MFC systems are commonly evaluated in terms of power and current densities (Rabaey and Verstraete, 2005; Logan, 2008)

Table 1 Electricity generating profile of MFCs fed with four different substrates after day 50

Substrate	AC-MFC Acetate		BP-MFC Butyrate/propionate		GL-MFC Glucose		SU-MFC Sucrose	
Reactor ID	a	b	a	b	a	b	b	c
Current (mA)[a]	5.6	5.9	4.4	4.7	4.8	5.0	4.8	4.6
± s.d.	± 0.2	± 0.2	± 0.1	± 0.2	± 0.2	± 0.2	± 0.2	± 0.3
Power density (mW m^{-2})[b]	80.7	91.0	51.2	55.9	60.7	63.2	63.2	62.0
Power output (W m^{-3})[c]	1.8	2	1.1	1.2	1.6	1.4	1.4	1.3
Current density (mA cm^{-2})[b]	0.065	0.069	0.052	0.054	0.056	0.058	0.058	0.057
Max. current density (mA cm^{-2})[b,d]								
2-month	0.222	0.198	0.227	0.221	0.190	0.190	0.204	0.181
3-month	0.279	0.256	0.313	0.298	0.282	0.289	0.282	0.283
CE (%)[e]	57	54	44	47	47	40	47	41
± s.d.	± 3	± 7	± 4	± 7	± 8	± 5	± 4	± 3

Abbreviation: CE, coulombic efficiency.
[a]Averaged current generation from day 55 to day 90 with 22 Ω external resistor.
[b]Power and current density were calculated per projected anode surface area.
[c]Power output per reactor was normalized by the reactor volume.
[d]Maximum current density was determined by linear sweep voltammetry at day 61–62 (2-month) and at day 91–92 (3-month).
[e]CE was calculated for each batch with 22 Ω external resistor, and averaged from day 55 to day 90.
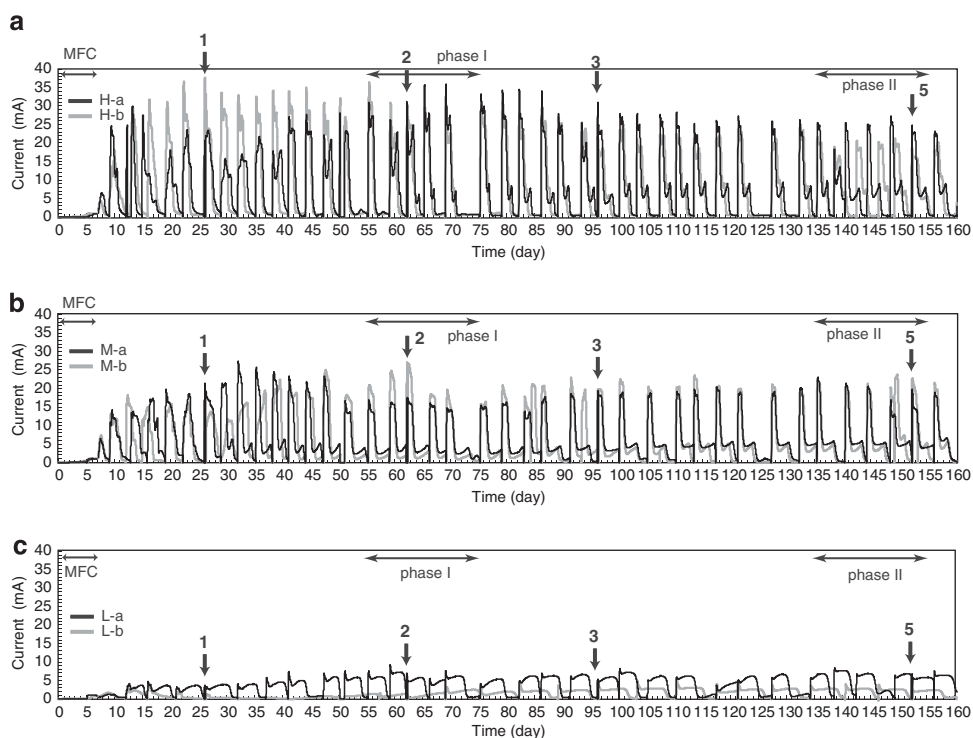
Figure 2 Electrical current generation in duplicate sucrose-fed SP reactors controlled to three different anode potentials. Duplicate SP reactors (**a** or **b**) were operated by controlling anode potential to $+100\,mV$ vs SHE (SP-H, panel **a**), $-50\,mV$ vs SHE (SP-M, panel **b**) and $-200\,mV$ vs SHE (SP-L, panel **c**). Arrows indicate anode biofilm sampling for DNA extraction and biomass determination.

Table 2 Electricity generating profile under SP operation with three controlled anode potentials

Anode potential (vs SHE)	SP-H $+100\,mV$		SP-M $-50\,mV$		SP-L $-200\,mV$	
Reactor ID	a	b	a	b	a	b
Phase I (day 55–75)						
Current (mA)[a]	32.2	31.2	16.2	21.1	6.9	2.5
± s.d.	± 3.5	± 2.6	± 1.0	± 4.2	± 1.8	± 1.0
Current density (mA cm^{-2})[b]	0.325	0.315	0.163	0.213	0.069	0.026
± s.d.	± 0.035	± 0.026	± 0.010	± 0.042	± 0.018	± 0.010
Max. current density (mA cm^{-2})[b,c]	0.270	0.305	0.215	0.323	0.219	0.027
CE (%)[d]	50	46	40	41	28	12
± s.d.	± 5	± 4	± 4	± 4	± 5	± 6
Phase II (day 135–155)						
Current (mA)[a]	24.2	19.9	20.0	21.7	7.0	3.5
± s.d.	± 2.9	± 1.4	± 2.0	± 1.0	± 1.0	± 0.7
Current density (mA cm^{-2})[b]	0.260	0.214	0.215	0.233	0.075	0.038
± s.d.	± 0.031	± 0.015	± 0.022	± 0.011	± 0.011	± 0.008
Max. current density (mA cm^{-2})[b,c]	0.297	0.246	0.297	0.358	0.235	0.044
CE (%)[d]	43	41	43	40	35	21
± s.d.	± 3	± 3	± 2	± 3	± 4	± 0

Abbreviations: CE, coulombic efficiency; SP, set-potential.
[a]Averaged maximum current generation for repeated batch exchanges during SP operation.
[b]Current density was calculated per projected anode surface area.
[c]Maximum current density was determined by linear sweep voltammetry at day 62 (2-month) and at day 152 (5-month).
[d]CE was calculated for each batch under SP operation, and averaged during the periods (phases I and II).

(Table 1). Electricity production was monitored as current vs time; however, the current production did not increase during the long-term MFC operations except when the external resistance was decreased (Figure 1). To better analyze the maximum available microbial current-generating properties apart from

968

system limitations, anode and cathode polarization curves were determined by linear sweep voltammetry (Tsujimura *et al.*, 2001). The curves clearly showed that the cathode polarization strongly affected the whole MFC system polarization; however, the anode polarization curves showed that anodic limiting current densities significantly increased from around $0.1\,\mathrm{mA\,cm^{-2}}$ to $0.3\,\mathrm{mA\,cm^{-2}}$ during the 3-month operation in all MFCs (Figures 3a–d). This result indicates that the potential microbial
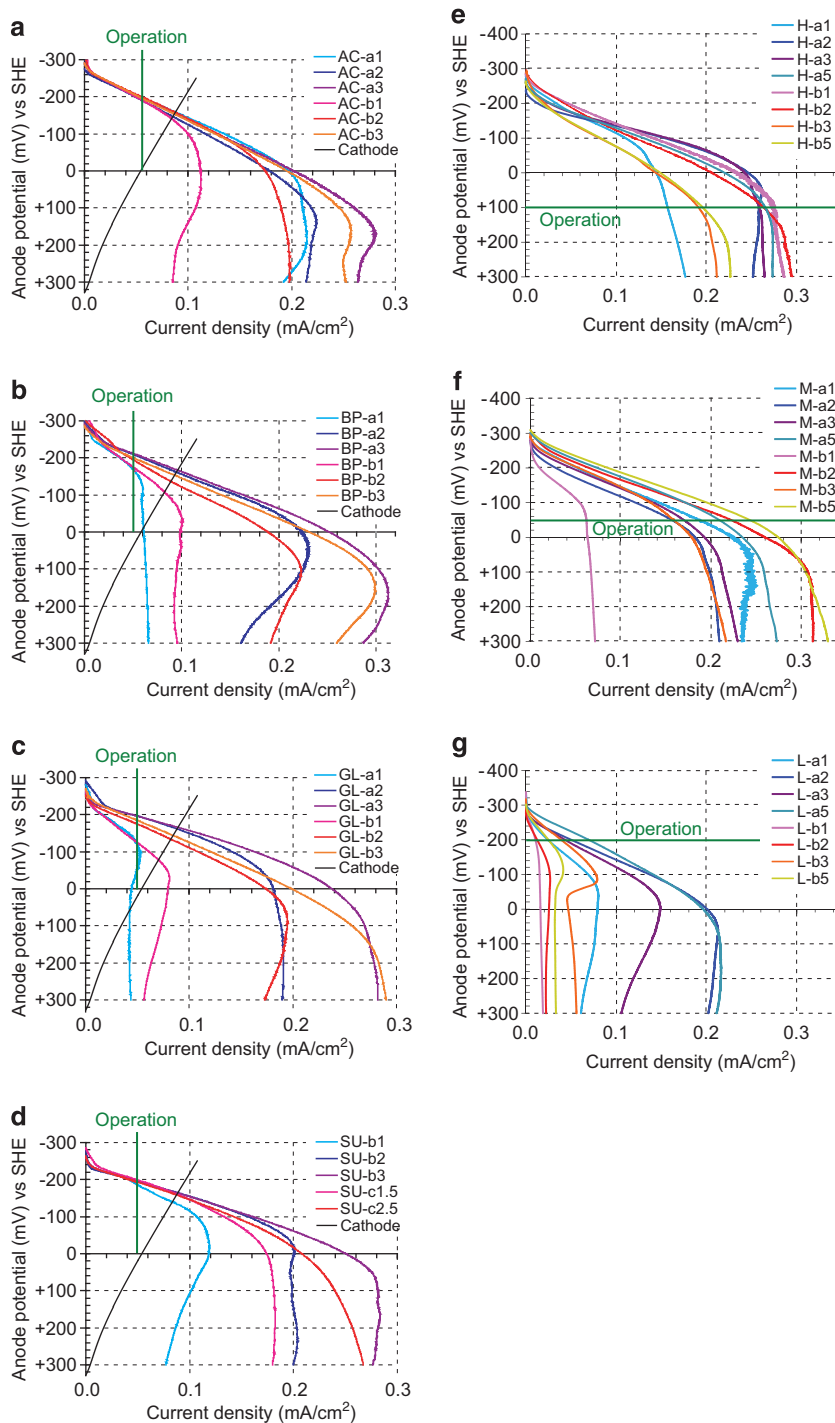

Figure 3 Anode polarization curves in the duplicate MFC and SP reactors during enrichment process. The anode polarization curves during the enrichment process of electricity-generating community in duplicate MFC and SP reactors (**a** or **b**) of AC-MFCs (**a**), BP-MFCs (**b**), GL-MFCs (**c**), SU-MFCs (**d**), SP-H (**e**), SP-M (**f**) and SP-L (**g**). The polarization curves were determined after collecting anode subsamples for microbial community analysis at 1 month, 2 months, 3 months and 5 months. Polarization curves were generated from linear sweep voltammetry at a scan rate of $0.5\,\mathrm{mV\,s^{-1}}$. Green lines indicate cathodic polarization curves for MFC reactors (**a–d**) or operating anode surface potentials for SP reactors (**e–g**).

EET activities were enhanced during the long-term MFC operation even though the operational currents were limited by the cathode polarization (Ishii et al., 2012).

On the other hand, the potentiostatic operation (SP reactors) artificially controls the anode potential, which enables the study of solely anodic EET processes without system and cathode limitations (Wagner et al., 2010). The polarization curves of the SP-H reactors indicate that potentiostatic operation at +100 mV vs SHE enabled the generation of maximum current density throughout the 5-month operational period (Figure 3e). The polarization curves of SP-M and SP-L reactors showed that their operational current densities (equal to EET rate) were strongly defined by the anode potentials (Figures 3f and g), which suggests that those microbial communities were affected by both anode potentials and the limited EET rates. The limiting current densities dynamics are also summarized in Tables 1 and 2.

Metabolic activity and coulombic efficiency
The substrate-consuming and by-product-producing trends were similar in the duplicate MFC reactors after day 55 (Figure 4 and Supplementary Figure S2), and in the duplicate SP reactors after 2 and 5 months (Figure 5 and Supplementary Figure S3). These observations indicate that the reactors achieved reproducible carbon metabolisms

associated with EET activities. In the AC-MFCs, acetate was steadily consumed. In the other MFC and SP reactors fed with more complex carbon sources, sugars, lactate and butyrate were consumed completely within 1 day after feeding. After these primary carbon sources were depleted, the microbial communities then began consuming acetate and propionate simultaneously with slightly lower electricity generation. Interestingly, acetate was consumed more rapidly than propionate for all reactors and the current generation was reduced significantly after acetate depletion, which indicates that acetate is an efficient and preferable substrate for the EET-active microbes. The ratio of by-products from primary sugar fermentation was variable for lactate, propionate and acetate in the GL/SU-MFCs and SP-H/M/L reactors, suggesting that microbial fermentation processes were affected by the EET operating conditions.

Electron recovery from substrate consumption was calculated as coulombic efficiency (Logan, 2008), which was found to be stable at ∼55% in the AC-MFCs, 10–30% in the SP-L reactors and
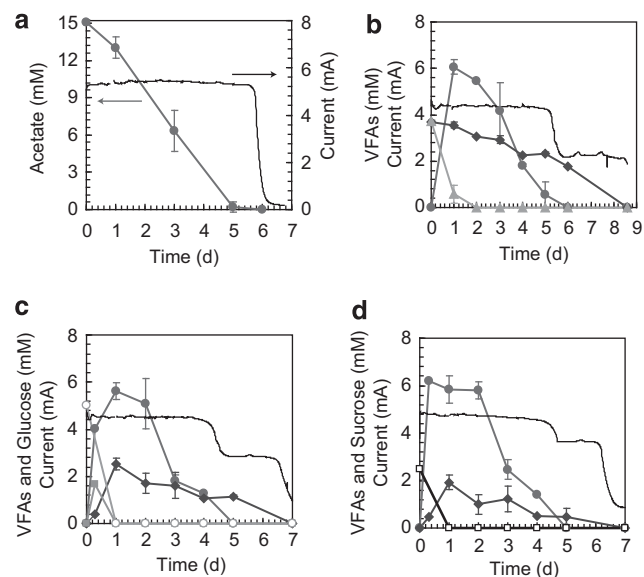

Figure 4 Exemplary current generation and substrate consumption rates in MFCs fed with different carbon sources. Typical batch cycle of reactor 'a' of AC-MFCs (**a**), BP-MFCs (**b**), GL-MFCs (**c**) and SU-MFCs (**d**) after the 3-month enrichment process. The black line indicates electric current (mA) with 22 Ω external resistance. Filled circles indicate acetate. Filled triangles indicate butyrate. Filled diamonds indicate propionate. Open circles indicate glucose. Filled squares indicate lactate. Open squares indicate sucrose.
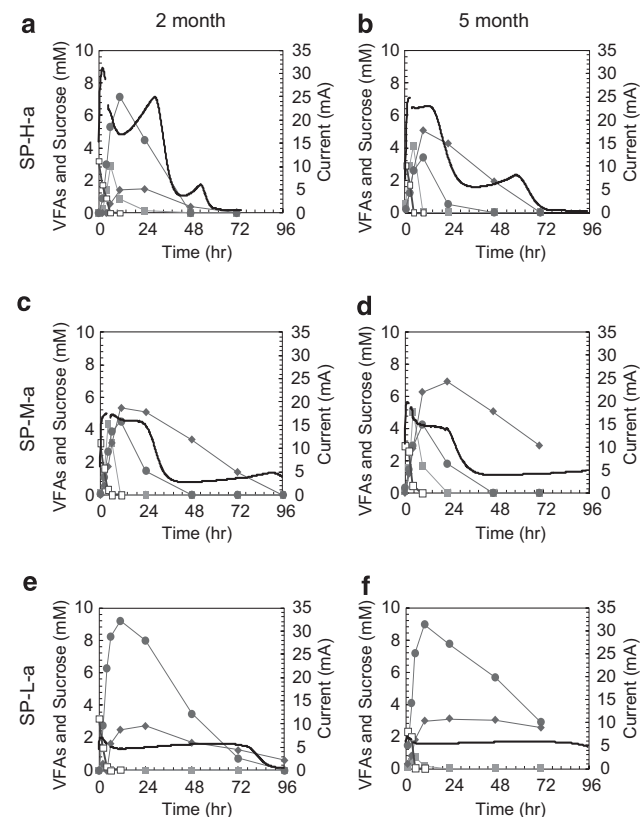

Figure 5 Exemplary current generation and substrate consumption rates in SP reactors with different anode potentials. Typical batch cycle of reactor 'a' under SP-H (**a** and **b**), SP-M (**c** and **d**) and SP-L (**e** and **f**) operation after the 2-month (**a**, **c** and **e**) and 5-month (**b**, **d** and **f**) enrichment process. The black line indicates electric current (mA) under anode potential controlled operations. Filled circles indicate acetate. Filled diamonds indicate propionate. Filled squares indicate lactate. Open squares indicate sucrose.

~45% in the other MFC and SP reactors (Tables 1 and 2). This indicates that approximately half of the electrons associated with the substrate degradation were directed to competing reactions such as oxygen respiration by the cathode biofilm, methanogenesis and/or biosynthesis.

Correlation between anode biomass and electricity production
The increase of limiting current density (Figure 3) can be attributed to two major factors: increasing biomass within the electrogenic biofilm and increasing per-biofilm biocatalytic activity through alterations of the microbial consortia. The biomass density of the anode biofilms showed consistent increases in all MFC and SP-M/L reactors (Figure 6), whereas that in SP-H reactors showed rapid saturation around 600 mg-protein cm^{-2} after 1-month operation. Per-biomass electron-donating rates, which were calculated using the limiting current densities and the biofilm densities (Ishii *et al.*, 2008), showed varying trends among the MFC and SP reactors (Figure 6).

In the MFC reactors, the per-biomass electron-donating (biocatalytic) rates changed considerably during early stages of biofilm formation (an average change of 48.3% from first month to second month)

and stabilized at later stages (an average change of 16.1% from second month to third month) likely due to diffusion limitations associated with thick biofilms and/or microbial community stability. The average biocatalytic rates after 3 months of operation were 336 ± 101 µmol-electron g-protein^{-1} min^{-1} for the AC/BP-MFCs and 179 ± 52 µmol-electron g-protein^{-1} min^{-1} for the GL/SU-MFCs (Figure 6a), which shows significantly different per-biomass EET activity ($P < 0.05$ by Student's *t*-test). The biomass densities in the AC/BP-MFCs were approximately half of those in the GL/SU-MFCs, indicating that fermentable substrates (glucose and sucrose) facilitated the development of thick biofilms consisting of electrode respirators and fermenters.

Biocatalytic rates were more variable in the SP reactors (Figure 6b). The SP-L-a reactor showed similar trends of both biofilm density and biocatalytic rates relative to the SU-MFCs, whereas the SP-L-b reactor appeared to take longer time to establish an EET-active biofilm. Even using the same fermentable substrate of sucrose, the average biocatalytic rates of the SP-H/M reactors (309 ± 118 µmol-electron g-protein^{-1} min^{-1}) showed significantly higher per-biomass anode reducing rates than the GL/SU MFCs as evaluated by Student's *t*-test ($P < 0.05$), suggesting that the SP-H/M as well as AC/BP-MFC reactors may have higher densities of
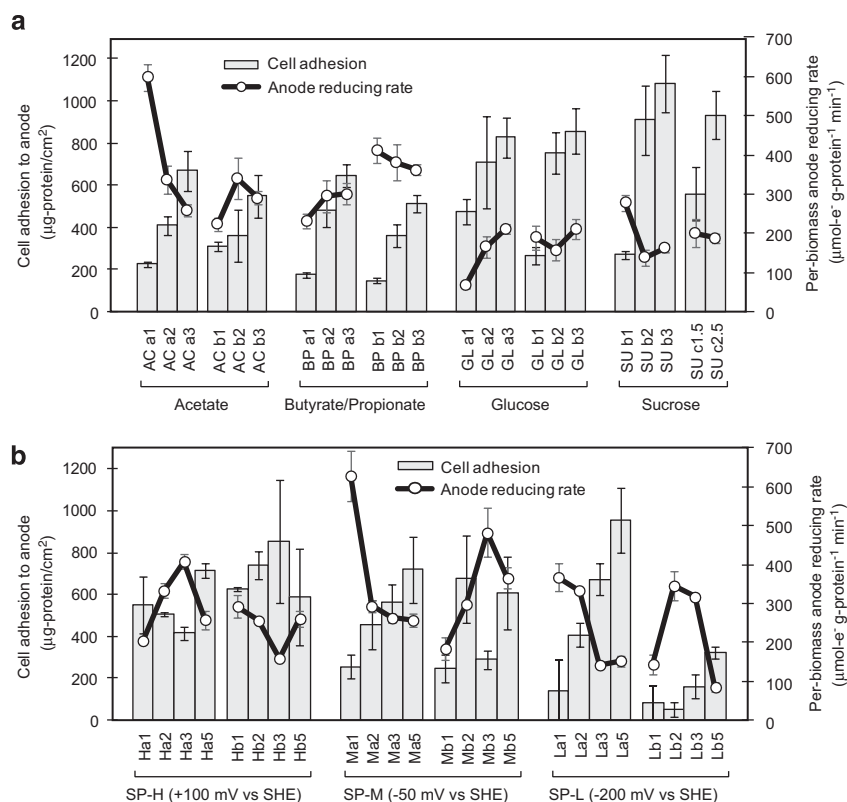
Figure 6 Biomass density and per-biomass anode reducing rate during enrichment process. Average cell adhesion to the anode and the per-biomass anode-reducing rates in duplicate MFCs (**a** and **b**) of AC-MFCs, BP-MFCs, GL-MFCs and SU-MFCs shown at 1 month, 2 months and 3 months of enrichment (panel **a**) and in duplicate SP reactors (**a** and **b**) of SP-H, SP-M and SP-L at 1 month, 2 months, 3 months and 5 months of enrichment (panel **b**). Error bars indicate standard deviations ($n > 3$).

electricity-generating microbes and/or more efficient EET-active microbes in their biofilms.

SEM observations of the AC/BP-MFC biofilms showed filamentous structures, whereas those of the GL/SU-MFC biofilms showed high cell densities (Supplementary Figure S4), which also indicates that the addition of sugar substrates established thick electrogenic biofilms. The anode electrodes in the SP-H/M reactors featured visually red biofilms after the 5-month period (Supplementary Figure S5). Redox-active red compounds such as *c*-type cytochromes are commonly observed in EET-active microbes such as *Geobacter* and *Shewanella* strains (Torres *et al.*, 2009; Summers *et al.*, 2010), which also suggests that SP-H/M biofilms had more EET-active microbes than those in the SP-L biofilms.

Microbial community composition
To analyze microbial community composition dynamics, we constructed 16S rRNA gene clone libraries of the lagoon sediment inoculum sources, periodically collected anode biofilm samples and several anolyte solution samples of sucrose-fed batch exchanges. The rarefaction curves showed that the abundance of phylotypes (classified as operational taxonomic units grouped using >99% cutoff value) in the anode communities was reduced throughout the enrichment process (Supplementary Figures S6 and S7). The Shannon's diversity index, Simpson diversity index and Chao-1 richness also support this trend (Supplementary Tables S1 and S2).

The phylum- or class-level community analyses clearly revealed that different substrate and anode potentials established and maintained different electrogenic communities (Figures 7a and b). Duplicate MFC and SP reactors (except for SP-L reactors) showed similar microbial communities, indicating reproducible enrichment processes of the electrogenic biofilms. The most abundant taxa of all the anode biofilms were *Deltaproteobacteria*, *Clostridia* and *Bacteroidetes*, whereas *Gammaproteobacteria* and *Bacilli* were only observed in fermentable sugar-fed MFC and SP reactors.

Under the MFC operations (Figure 7a), *Deltaproteobacteria* (genera *Desulfuromonas* and *Geobacter*) and *Bacteroidetes* were highly abundant in the AC-MFCs, whereas *Deltaproteobacteria* (genus *Geobacter*) and *Clostridia* (genera *Syntrophomonas* and *Acetoanaerobium*) were the relatively abundant in the BP-MFCs. In contrast, the fermentable sugar-fed MFCs (GL/SU-MFCs) showed that *Gammaproteobacteria* (genera *Tolumonas* and *Aeromonas*) comprised 70% of the clone libraries, whereas *Deltaproteobacteria* (genus *Geobacter*) occupied only 10% of the enriched microbial communities. Under the SP operation (Figure 7b), SP-L reactors showed similar trends to the sucrose-fed MFCs (SU-MFCs), whereas SP-H and SP-M reactors appeared to feature genus *Geobacter* and class *Bacilli* more abundantly than the other sucrose-fed reactors.

In addition, the microbial community compositions were compared between anode biofilms and suspended cells in the sucrose-fed MFC and SP reactors (Supplementary Figure S8). The results clearly show that *Deltaproteobacteria* was rarely observed in solution, and that *Bacilli* and/or *Gammaproteobacteria* were highly abundant in solution. This result indicates that *Deltaproteobacteria* was strongly associated with the anode electrode, but that *Bacilli* and *Gammaproteobacteria* were able to grow without direct electrode reducing processes and may have preferentially contributed to sucrose fermentation in both the electrode biofilm and anolyte solution.

Microbial community dynamics
A multidimensional scale plot created based on family-level taxonomy clearly showed that the electrogenic communities differed substantially from the original inoculum source, and organized based on the type of substrate fed to the MFCs, or surface potentials of the SP anodes (Figure 7c). Community similarities in the MFCs are in three distinct clusters that feature the AC-MFCs, BP-MFCs and fermentable sugar-fed MFCs. Even with the sugar-fed operation, SP-H and SP-M reactors showed distinct clusters from the SU/GL-MFCs. Interestingly, the SP-L reactors clustered similarly to those of the SU/GL-MFCs at 5-month period, although the SP-L-b reactor community did not cluster with any of the other groups during the initial 3-month operation.

A heat map table of Sørensen's similarity coefficients created based on operational taxonomic units is also used for statistically calculating the microbial community similarities among operational conditions or temporal differences (Supplementary Figure S9), which indicates the continuity of anode community establishment with time, as well as high similarity between duplicate GL-MFC and SU-MFC communities within MFC operations, and the SP-H and SP-M communities within SP operations.

Fermenting and electricity-generating bacteria
Figure 8 shows the phylotypes (>99% cutoff value) that were frequently identified within the clone libraries from each electrogenic biofilm. The minor (that is, lower relative abundance) phylotypes are summarized in Supplementary Tables S3 and S4. The phylotypes affiliated to highly abundant taxa are independently addressed below:

(i) Deltaproteobacteria. Eleven different *Deltaproteobacteria* phylotypes were found to be relatively abundant within all the electrogenic communities. One *Desulfuromonas* (Des1) and one *Geobacter* (Ac3) phylotype were highly abundant in the AC-MFCs, whereas four more *Geobacter* phylotypes (Geo1, Geo2, Gl1 and Gl2) were observed in the BP-MFCs. The GL/SU-MFC and SP-L-a reactors
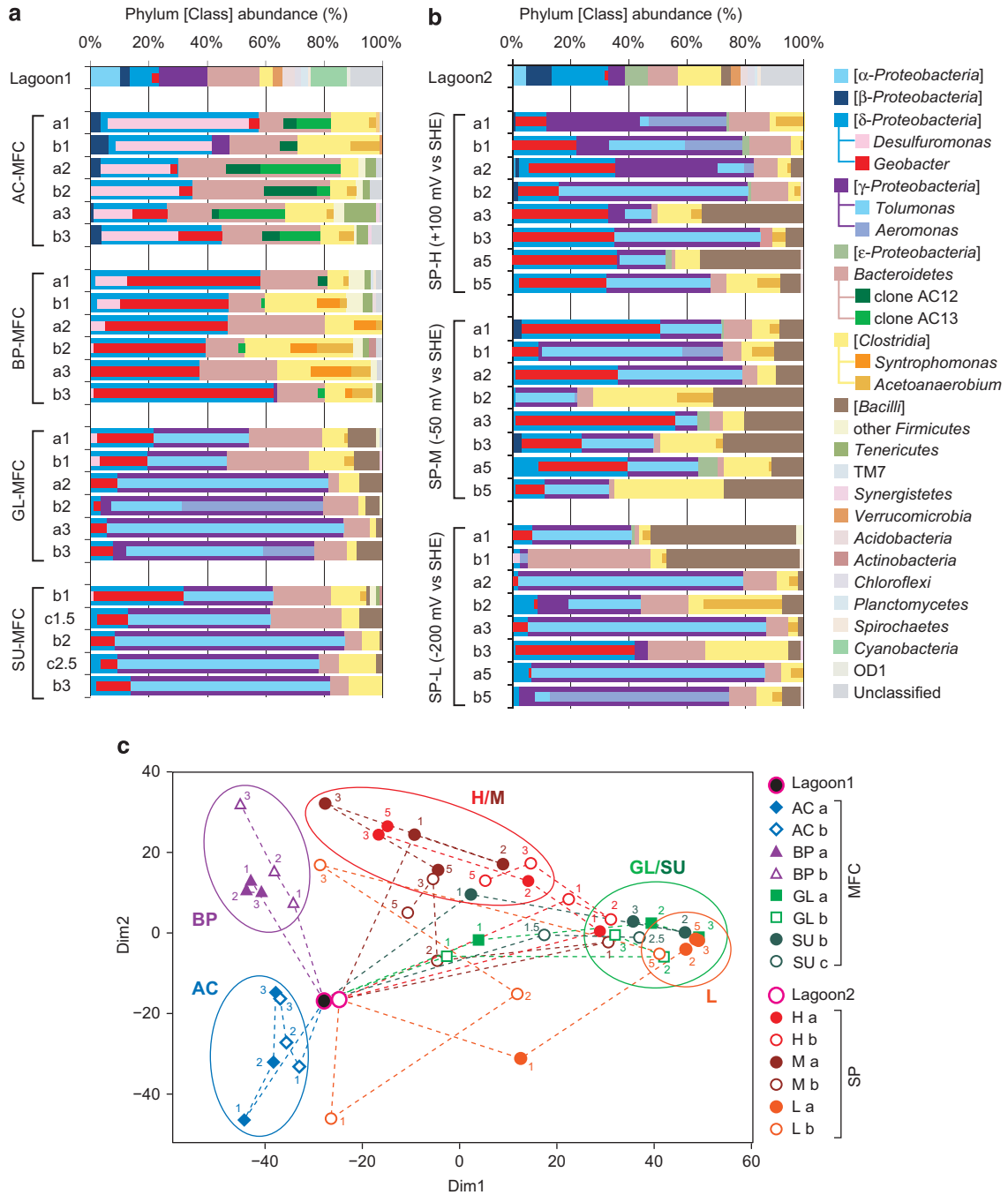
Figure 7 Taxonomic distributions of 16S rRNA community profile within anode electrogenic biofilms. (**a**) The phylum or class-level taxonomic profiles for the duplicate MFC anode biofilms (**a** and **b**) fed with four different substrates at 1 month, 2 months and 3 months of enrichment, and the original inoculum source of lagoon sediment (Lagoon 1). Phylum *Proteobacteria* and *Firmicutes* are divided into class-level taxonomies. Six dominant genera and two *Bacteroidetes* sp. phylotypes in the communities are shown in inner bars. (**b**) The taxonomic profiles for the duplicate SP anode biofilms (**a** and **b**) controlled to three different anode potentials at 1 month, 2 months, 3 months and 5 months of enrichment, and the original inoculum source of lagoon sediment (Lagoon 2). (**c**) Multidimensional scale plot comparing bacterial communities based on family-level taxonomy. The labels for operational conditions are depicted on the right side of the panel (reactor 'a' for solid labels or 'b' for open labels). The communities were taxonomically characterized at 1 month, 2 months, 3 months and 5 months as indicated by the numbers above the symbols.

showed similar phylotype-level trends. The early stages of the sugar-fed enrichment process showed four relatively abundant phylotypes (Des1, Geo1, Gl1 and Gl2), which were also observed in the AC/BP-MFCs. However, the most relatively abundant

phylotype shifted to a different *Geobacter* (Gl15) in the later stages of GL/SU-MFC operation.

Interestingly, the higher current-generating SP enrichments revealed different phylotype trends. SP-M reactors also showed shifts of the dominant
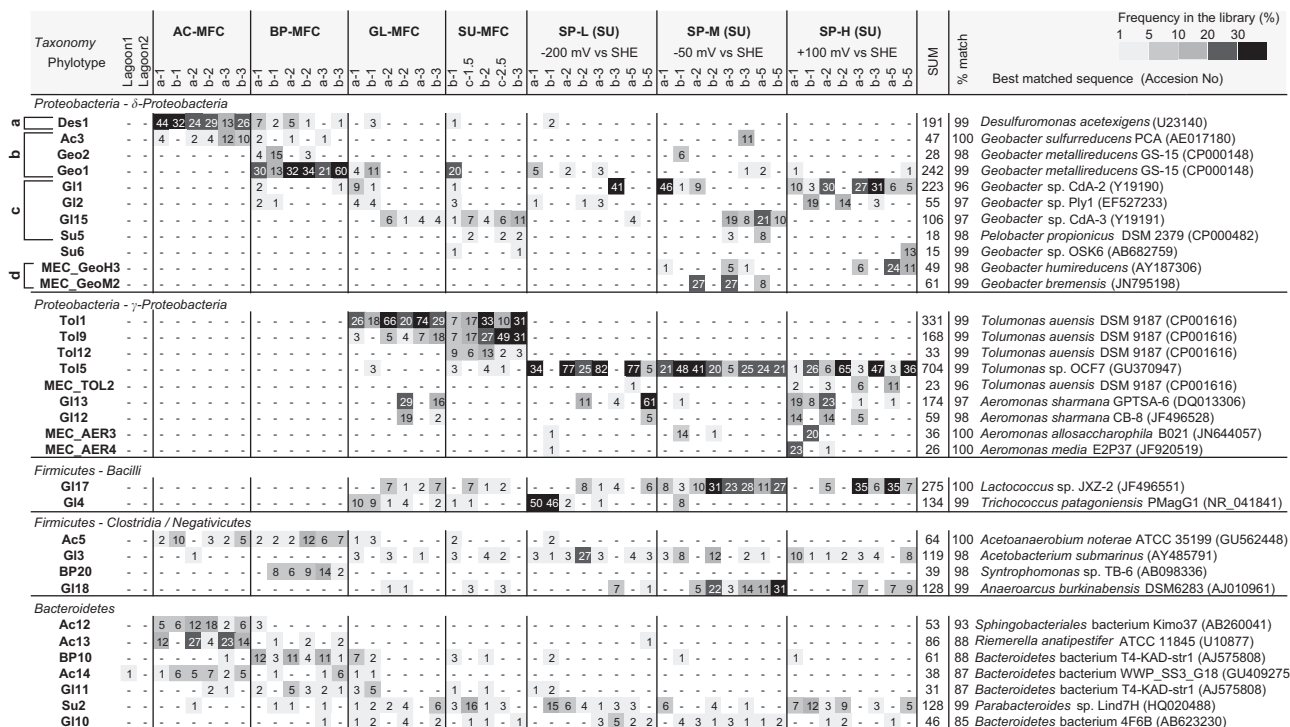
Figure 8 Heatmap table of major phylotypes in the anodic bacterial communities. The major phylotypes were selected as those with frequencies that summed to over 15% in all 49 clone libraries. The calculation of frequency (%) was conducted based on Supplementary Tables S3 and S4. *Desulfuromonadales* sub-clade of *Deltaproteobacteria* phylotypes were described above the phylotype name as (a) *D. acetoxidans* clade, (b) *G. metallireducens* clade, (c) *Geobacter* subsurface clade 2 and (d) *Geobacter* subsurface clade 1.

Taxonomy / Phylotype	SUM	% match	Best matched sequence (Accesion No)
Proteobacteria - δ-Proteobacteria			
(a) Des1	191	99	*Desulfuromonas acetexigens* (U23140)
(b) Ac3	47	100	*Geobacter sulfurreducens* PCA (AE017180)
(b) Geo2	28	98	*Geobacter metallireducens* GS-15 (CP000148)
(b) Geo1	242	99	*Geobacter metallireducens* GS-15 (CP000148)
(c) Gl1	223	96	*Geobacter* sp. CdA-2 (Y19190)
(c) Gl2	55	97	*Geobacter* sp. Ply1 (EF527233)
(c) Gl15	106	97	*Geobacter* sp. CdA-3 (Y19191)
(c) Su5	18	98	*Pelobacter propionicus* DSM 2379 (CP000482)
(c) Su6	15	99	*Geobacter* sp. OSK6 (AB682759)
(d) MEC_GeoH3	49	98	*Geobacter humireducens* (AY187306)
(d) MEC_GeoM2	61	99	*Geobacter bremensis* (JN795198)
Proteobacteria - γ-Proteobacteria			
Tol1	331	99	*Tolumonas auensis* DSM 9187 (CP001616)
Tol9	168	99	*Tolumonas auensis* DSM 9187 (CP001616)
Tol12	33	99	*Tolumonas auensis* DSM 9187 (CP001616)
Tol5	704	99	*Tolumonas* sp. OCF7 (GU370947)
MEC_TOL2	23	96	*Tolumonas auensis* DSM 9187 (CP001616)
Gl13	174	97	*Aeromonas sharmana* GPTSA-6 (DQ013306)
Gl12	59	98	*Aeromonas sharmana* CB-8 (JF496528)
MEC_AER3	36	100	*Aeromonas allosaccharophila* B021 (JN644057)
MEC_AER4	36	100	*Aeromonas media* E2P37 (JF920519)
Firmicutes - Bacilli			
Gl17	275	99	*Lactococcus* sp. JXZ-2 (JF496551)
Gl4	134	99	*Trichococcus patagoniensis* PMagG1 (NR_041841)
Firmicutes - Clostridia / Negativicutes			
Ac5	64	100	*Acetoanaerobium noterae* ATCC 35199 (GU562448)
Gl3	119	98	*Acetobacterium submarinus* (AY485791)
BP20	39	98	*Syntrophomonas* sp. TB-6 (AB098336)
Gl18	128	99	*Anaeroarcus burkinabensis* (AJ010961)
Bacteroidetes			
Ac12	53	93	*Sphingobacteriales* bacterium Kimo37 (AB260041)
Ac13	86	88	*Riemerella anatipestifer* ATCC 11845 (U10877)
BP10	61	88	*Bacteroidetes* bacterium T4-KAD-str1 (AJ575808)
Ac14	38	87	*Bacteroidetes* bacterium WWP_SS3_G18 (GU409275)
Gl11	31	87	*Bacteroidetes* bacterium T4-KAD-str1 (AJ575808)
Su2	128	85	*Parabacteroides* sp. Lind7H (HQ020488)
Gl10	46	85	*Bacteroidetes* bacterium 4F6B (AB623230)

Geobacter phylotype from Gl1 to Gl15; however, other *Geobacter* phylotypes (MEC_GeoM2, SU5 and MEC_GeoH3) were also observed during the operation. SP-H reactors featured five different *Geobacter* phylotypes, but never showed the phylotype Gl15. The phylotypes Gl1 and Gl2 were highly abundant in the SP-H reactors during the initial 3 months, but by month 5, the abundant *Geobacter* phylotype shifted to MEC_GeoH3. These combined results indicate that different types of *Geobacter/Desulfuromonas* phylotypes were enriched in the electrogenic biofilms depending on the substrates in the MFC reactors and the anode surface potentials in the SP reactors. In addition, the shifts of dominant *Deltaproteobacterial* phylotypes were a common occurrence throughout the community development. The phylogenetic positions of those phylotypes are shown in Figure 9a.

(ii) Gammaproteobacteria. All observed *Gammaproteobacteria* phylotypes were related to genera *Tolumonas* and *Aeromonas*, which were only found in the sugar-fed MFC and SP reactors. Those phylotypes were remarkably abundant in the GL/SU-MFCs and SP-L reactors, and also observed in the anolyte solutions (Supplementary Tables S3 and S5), suggesting that the phylotypes had an important role in fermentation in the biofilm and planktonic populations. The phylogenetic positions of those phylotypes are shown in Figure 9b.

(iii) Firmicutes (Clostridia and Bacilli). Four *Firmicutes* phylotypes were frequently observed in the sugar-fed MFC/SP reactors. The *Trichococcus* phylotype Gl4 was found in earlier stages of the development processes, but the abundant phylotypes shifted to the *Lactococcus* phylotype Gl17 and *Anaeroarcus* phylotype Gl18. Those two phylotypes were also highly abundant in the anolyte solution of SP-H/M reactors (Supplementary Table S5), which suggests that the phylotypes had an important role in consuming sugar compounds under higher current-producing conditions. Another two *Clostridia* phylotypes (Ac5 and BP20) were mainly observed in AC/BP-MFCs, suggesting the contribution to acetate, propionate and/or butyrate metabolism in the communities. The phylogenetic positions of those phylotypes are shown in Supplementary Figure S10.

(iv) Bacteroidetes. Two *Bacteroidetes* phylotypes Su2 and Gl10 were consistently found in all the sugar-fed MFC/SP reactors, whereas five other phylotypes were mainly found in the AC/BP-MFCs. The phylotypes Ac12 and Ac13 were highly abundant in the AC-MFCs (Figure 7a), and phylotype BP10 was relatively abundant in the BP-MFCs.
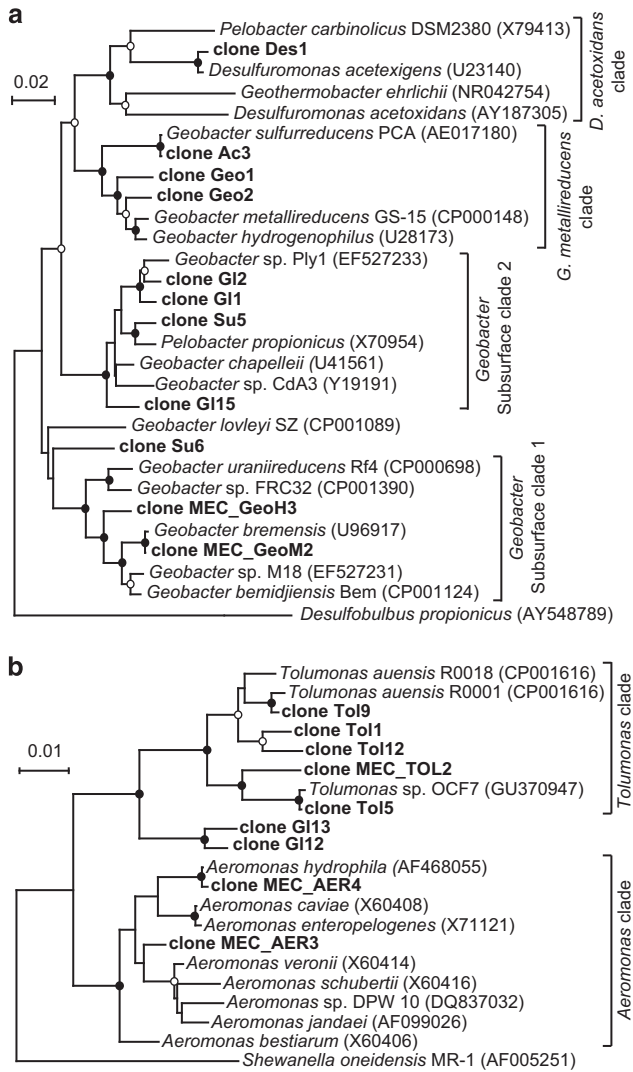
a

b

Figure 9 Neighbor-joining phylogenetic trees showing positions of major phylotypes representing anodic microbial populations. Panel **a** for order *Desulfuromonadales*, and panel **b** for family *Aeromonadaceae*. Branch points supported with bootstrap values (100 trials) of >90% are indicated with closed circles, whereas those between 70 and 90% are indicated with open circles. Accession numbers of reference sequences are indicated in parentheses.

These results suggest that the *Bacteroidetes* phylotypes had a role in the anode biofilms, and have substrate preference in the EET-active communities. The phylogenetic positions of those phylotypes are shown in Supplementary Figure S11.

Correlations between environmental factors and microbial taxa

CCA is a comparative evaluation tool that can diagram correlations between key environmental variables and associated species (phylotype) compositions (ter Braak, 1986). Figure 10a shows the associations between metabolite variations in all MFC/SP reactors (maximum concentrations during each batch shown in Figures 4 and 5 and
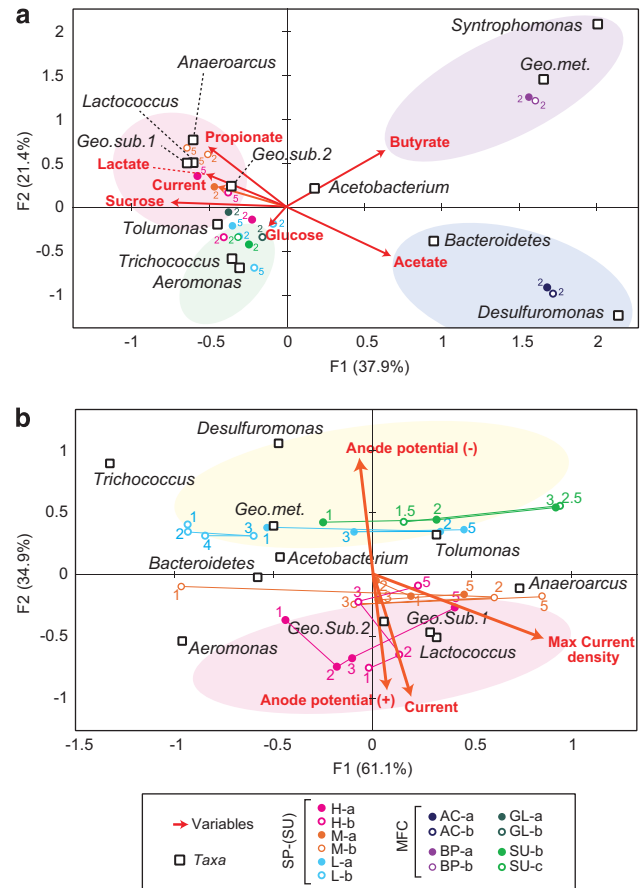
a

b

Figure 10 CCA diagram correlating microbial taxa and the environmental factors. CCA diagrams reveal the relationships between operational variables and microbial taxa in MFC/SP reactors. Panel **a** shows relationships associated with metabolic variables indicated as red arrows, and panel **b** shows relationships associated with electrochemical variables indicated as orange arrows. Solid (for reactor 'a') and open (for reactor 'b') circles indicate samples for microbial community analyses of MFC/SP reactors (with different colors summarized in legend panel). Sampling months are indicated by the numbers close to the symbols. The 12 most highly abundant genus-level taxa are shown as open squares, and genus *Geobacter* is divided into the three described sub-clades (Geo. met., *Geobacter metallireducens* clade; Geo. Sub. 1, *Geobacter* subsurface clade 1; Geo. Sub. 2, *Geobacter* subsurface clade 2). Phylum *Bacteroidetes* is also shown as an open square; however, it represents all phylotypes associated with *Bacteroidetes*.

Supplementary Figures S2 and S3) observed as the vectors and 12 highly abundant genus-level taxa in the microbial communities. Phylum *Bacteroidetes* represents all associated phylotypes, and genus *Geobacter* was further divided into the three sub-clades shown in Figure 9a. Within the three *Geobacter* sub-clades, both *Geobacter* subsurface clades 1 and 2 were strongly correlated with current generation associated with lactate, sucrose and propionate metabolism. On the other hand, the *Geobacter metallireducens* clade was strongly associated with butyrate metabolism, along with genus *Syntrophomonas*. Genus *Desulfuromonas* and phylum *Bacteroidetes* were most closely associated

with acetate metabolism. Genera *Tolumonas*, *Trichococcus* and *Aeromonas* were related to sucrose and/or glucose metabolisms; however, genus *Lactococcus* and *Anaeroarcus* were strongly associated with current generation along with lactate, propionate and sucrose metabolism as indicated by the close clustering to the variable vectors.

Figure 10b shows associations between electrochemical variables (operational current, maximum current density and anode electrode potential) in the sucrose-fed MFC/SP reactors and the 12 highly abundant taxa described above. The anode potential in SU-MFCs was estimated as − 220 mV vs SHE for the analysis. The operational current and anode potential vectors were nearly aligned along the same axes; however, the maximum current density vector indicates that biocatalytic activity was a more unique variable that was strongly associated with genus *Anaeroarcus*, and also enrichment time (months). *Geobacter* subsurface clades 1 and 2, *Lactococcus*, and *Aeromonas* were related to electropositive anode potentials with higher current generation, whereas the *G. metallireducens* clade, *Desulfuromonas*, *Tolumonas* and *Trichococcus* were associated with electronegative anode potentials with lower current generation. Within the 12 taxa, *Geobacter* subsurface clade 1 and *Lactococcus* were most closely related to each other based on operational variables that were observed in the SP-H/M reactors. These results provide a more detailed description of how electrode surface potential, whole community EET rates (current generation) and substrate/secondary metabolite consumption contribute as selective pressures for community development in EET-active biofilms.

Discussion

In this study, a variety of substrate and anode potential conditions were used to examine the relationships between electrochemical performance, metabolic activities and EET-active microbial community development. Higher per-biomass EET rates were observed in the volatile fatty acid-fed MFC reactors and also in SP-H/M reactors relative to sugar-fed MFCs and SP-L reactors (Figure 6). At the early stages of the operations, some reactors showed decreased per-biomass biocatalytic rates with increasing biomass density of the electrogenic biofilm. This trend suggests that mono-layers or thin biofilms had more effective electrogenic activity due to improved direct electron transport from microbial cells to the electrode, and also better substrate accessibility and proton diffusion (Yi *et al.*, 2009; McLean *et al.*, 2010). The microbial communities with the higher per-biomass EET rates also featured a higher relative abundance of well-known EET-active microbial groups, *Geobacter* and *Desulfuromonas* (Figures 7a and b), indicating that the taxonomic groups have an important role in EET reactions as proposed previously (Kiely *et al.*, 2011).

As for fermenters, *Bacilli*, *Clostridia* and *Gammaproteobacteria* presumably performed sugar fermentation because these strains were observed more frequently in both the anode and anolytes of sugar-fed reactors (Figures 7a and b, Supplementary Figure S8), and also their close relatives are known as sucrose fermenters (Fischer-Romero *et al.*, 1996; Cho *et al.*, 2008). Some of the fermenting *Clostridium*, *Aeromonas* and *Tolumonas* strains have been reported as EET-active fermenters (Park *et al.*, 2001; Pham *et al.*, 2003; Chung and Okabe, 2009; Luo *et al.*, 2013), suggesting the *Clostridium*, *Aeromonas* and *Tolumonas* phylotypes in our sugar-fed reactors might conduct EET reactions directly. The microbial metabolic functions are further discussed in Supplementary Discussion.

A comparison of family-level population dynamics revealed that different carbon substrates (electron donor) and anode potentials (electron acceptor) conferred different selective pressures during the establishment of EET-active communities (Figures 7a and b). However, fermentative substrates (GL/SU-MFC) and limiting electron acceptors (SP-L) appear to induce similar selective pressures on microbial communities (Figure 7c). Comparisons of various electrochemical and metabolic parameters associated with these three reactor sets revealed that the EET rates represented by operational current generation were similar at ∼ 7 mA (Tables 1 and 2). In addition, similarities between microbial community dynamics and electrochemical performance were also observed for the SP-H and SP-M reactors, which both generated ∼ 20 mA of current (Figure 2) and had similar microbial communities after 3 months of operation (Figures 7b and c). These results imply that EET rates have a huge impact on the family-level microbial community development of EET-active microbial communities.

The CCA diagrams clearly indicate that fermenting *Lactococcus*, *Anaeroarcus* and *Aeromonas* strains preferred higher EET rate conditions under electropositive anode surface potentials (SP-H/M reactors), whereas *Tolumonas* and *Trichococcus* strains were correlated with lower EET rate conditions under electronegative surface potentials (SU/GL-MFCs and SP-L reactors) (Figures 8 and 10). Interestingly, these potential fermentor strains were also observed in the anolyte solution under each operational condition (Supplementary Figure S8 and Supplementary Table S5). These observations suggest that these strains were not likely associated with direct electron transfer to the electrode; however, they may have interacted with the electrode through indirect EET and/or had a close association with the electrode because of the rapid consumption of fermentation by-products by the electrode respiring portion of the communities. These results implied that the EET rates in microbial systems define the fermenter population, most likely, because the consumption of the fermentation by-products (acetate, propionate and H_2) is coupled with electrode respiration rates of the electrogenic microbes.

Comparison of the phylotype-level taxonomic composition of the potential electrogens, affiliated to families *Geobacteraceae* and *Desulfuromonadaceae,* showed more diverse phylotypes related to the operational conditions (Figure 8). Phylogenetic analyses of *Geobacter* strains (Figure 9a) revealed that phylotypes classified within *G. metallireducens* clade were mainly observed in AC/BP-MFCs and early stages of sugar-fed MFC and SP-L reactors. These results suggest that the well-known EET-active *Geobacter* strains affiliated to the *G. metallireducens* clade prefer electronegative anode potentials and simple volatile fatty acid compounds (Figure 10). However, the early stages of SP-H/M reactors abundantly showed phylotypes classified within *Geobacter* subsurface clade 2, suggesting that surface potential is the key factor for selection of *Geobacter* strains during the early stages of biofilm formation (Figure 10b). The results may also imply that microbial adaption to electrode and/or metal reduction are affected by outer-membrane proteins such as *c*-type cytochromes, which are known to be involved with *Geobacter* EET processes and are strain-specific (Butler *et al.*, 2010). Our previous metatranscriptomic analyses indicated that *Desulfuromonadales* (including genus *Geobacter*) and *Desulfobulbus* strains responded to surface potential changes by different gene expression levels of outer membrane *c*-type cytochromes. These significant changes in gene transcription were related to increases in EET rates when exposed to SP electropositive conditions (Ishii *et al.*, 2013). These data suggest that different *c*-type cytochromes may define an affinity for microbial electron transfer to substrates with specific surface potentials. The *G. metallireducens* clade includes well-known electricity generators that utilize acetate, hydrogen, alcohols or monoaromatic compounds as energy sources (Bond *et al.*, 2002; Bond and Lovley, 2003) and uses different types of outer-membrane multi-heme *c*-type cytochromes for conducting EET process with different forms of solid iron featuring specific surface potentials (Kato *et al.*, 2013). The *Geobacter* subsurface clades strains are not often observed in electrogenic biofilms (Kato *et al.*, 2010; Nercessian *et al.*, 2012), and are predominantly observed in subsurface sediments that include a diversity of solid particles having different surface potentials (Holmes *et al.*, 2007). This might be a reason why the *Geobacter* subsurface clade 2 strains were selectively adapted to electropositive surface potentials in the early stages of SP-H/M reactors.

At the later stages of operation, the dominant *Geobacter* phylotypes shifted in all sugar-fed MFC/SP reactors. In the SU/GL-MFCs and SP-L-a reactors with lower EET rates, phylotypes classified within *Geobacter* subsurface clade 2 became more abundant than *G. metallireducens* clade, accompanied with the increase of *Tolumonas* strains (Figure 8). On the other hand, in the SP-H/M reactors with higher current generation, phylotypes classified within *Geobacter*

subsurface clade 1 began increasing the relative abundance in addition to *Geobacter* subsurface clade 2, accompanied with the increased abundance of a *Lactococcus* strain. The CCA diagrams indicate that the *Geobacter* subsurface clade 1 was highly associated with electropositive anode potentials and higher current generation (Figure 10b) as well as with lactate and propionate metabolism (Figure 10a). Interestingly, the diagrams also reveal that the *Geobacter* subsurface clade 1 strongly correlates with the lactate-metabolizing genus *Lactococcus* (Cho *et al.*, 2008). This association suggests the establishment of a symbiotic relationship between these genera so that sucrose is consumed via lactate and/or propionate production, and preferentially occurs under conditions with higher current generation (SP-H/M reactors) at the later enrichment stages. The *Geobacter* phylotype trends are further discussed in Supplementary Discussion.

In conclusion, this study revealed that strain-level selection of electrogenic organisms is highly correlated to specific surface potentials, and that EET rates may also define symbiotic relationships between solid-surface respiring and fermentative microbes. Different *Geobacter* strains were found to be associated with operational reactor conditions, suggesting that each *Geobacter* strain may have a defined range of surface potentials and carbon substrates that are required for life-sustaining EET reactions. Both *Desulfuromonas* and *G. metallireducens* clades, which are well-known electrogenic microbes, were associated with lower surface potentials and less current generation, whereas *Geobacter* subsurface clades 1 and 2 were associated with higher surface potentials and greater current generation. A clade-specific association to surface potentials has never been described for the genus *Geobacter*.

During EET-active community development, *Geobacter* phylotype shifts occurred in all sugar-fed reactors, and the *Geobacter* population became more diverse especially under higher current conditions. In addition, a clear association between communities of fermenters (*Lactococcus* and *Anaeroarcus*) and electrogens (*Geobacter* subsurface clade 1) was observed under electropositive surface potential conditions with higher EET rates. This suggests that diverse *Geobacter* populations, including *Geobacter* subsurface clades 1 and 2, may form symbiotic relationships with fermentative community members to better adapt to respiring solid substrates using more complex substrates like sucrose. These findings are important for understanding the fundamental nature of how EET-active communities are established; and provide new knowledge about the specific selective pressures that correlate to strain-level adaptation and cooperation within EET-active biofilms.

Conflict of Interest

The authors declare no conflict of interest.

Acknowledgements

References

Aelterman P, Freguia S, Keller J, Verstraete W, Rabaey K. (2008). The anode potential regulates bacterial activity in microbial fuel cells. *Appl Microbiol Biotechnol* **78**: 409–418.

Bond DR, Holmes DE, Tender LM, Lovley DR. (2002). Electrode-reducing microorganisms that harvest energy from marine sediments. *Science* **295**: 483–485.

Bond DR, Lovley DR. (2003). Electricity production by *Geobacter sulfurreducens* attached to electrodes. *Appl Environ Microbiol* **69**: 1548–1555.

Butler JE, Young ND, Lovley DR. (2010). Evolution of electron transfer out of the cell: comparative genomics of six *Geobacter* genomes. *BMC Genomics* **11**: 40.

Canfield DE, Thamdrup B, Hansen JW. (1993). The anaerobic degradation of organic matter in Danish coastal sediments: iron reduction, manganese reduction, and sulfate reduction. *Geochim Cosmochim Acta* **57**: 3867–3883.

Cheng S, Liu H, Logan BE. (2006). Increased performance of single-chamber microbial fuel cells using an improved cathode structure. *Electrochem Commun* **8**: 489–494.

Cho SL, Nam SW, Yoon JH, Lee JS, Sukhoom A, Kim W. (2008). *Lactococcus chungangensis* sp. nov., a lactic acid bacterium isolated from activated sludge foam. *Int J Syst Evol Microbiol* **58**: 1844–1849.

Chung K, Okabe S. (2009). Characterization of electrochemical activity of a strain ISO2-3 phylogenetically related to *Aeromonas* sp. isolated from a glucose-fed microbial fuel cell. *Biotechnol Bioeng* **104**: 901–910.

Cornell RM, Schwertmann U. (2003). The Iron OxidesWilley-VCH Verlagsgesellschaft: Weinheim, Germany.

DeLong EF. (1992). Archaea in coastal marine environments. *Proc Natl Acad Sci USA* **89**: 5685–5689.

Dubois M, Gilles KA, Hamilton JK, Rebers PA, Smith F. (1979). Colorimetric method for the determination of sugars and related substances. *Anal Chem* **28**: 350–356.

Fan Y, Sharbrough E, Liu H. (2008). Quantification of the internal resistance distribution of microbial fuel cells. *Environ Sci Technol* **42**: 8101–8107.

Fischer-Romero C, Tindall BJ, Juttner F. (1996). *Tolumonas auensis* gen. nov., sp. nov., a toluene-producing bacterium from anoxic sediments of a freshwater lake. *Int J Syst Bacteriol* **46**: 183–188.

Freguia S, Teh EH, Boon N, Leung KM, Keller J, Rabaey K. (2010). Microbial fuel cells operating on mixed fatty acids. *Bioresour Technol* **101**: 1233–1238.

Holmes DE, O'Neil RA, Vrionis HA, N'Guessan LA, Ortiz-Bernad I, Larrahondo MJ et al. (2007). Subsurface clade of *Geobacteraceae* that predominates in a diversity of Fe(III)-reducing subsurface environments. *ISME J* **1**: 663–677.

Hong YY, Call DF, Werner CM, Logan BE. (2011). Adaptation to high current using low external resistances eliminates power overshoot in microbial fuel cells. *Biosens Bioelectron* **28**: 71–76.

Humayoun SB, Bano N, Hollibaugh JT. (2003). Depth distribution of microbial diversity in Mono Lake, a meromictic soda lake in California. *Appl Environ Microbiol* **69**: 1030–1042.

Ishii S, Watanabe K, Yabuki S, Logan BE, Sekiguchi Y. (2008). Comparison of electrode reduction activities of *Geobacter sulfurreducens* and an enriched consortium in an air-cathode microbial fuel cell. *Appl Environ Microbiol* **74**: 7348–7355.

Ishii S, Suzuki S, Norden-Krichmar TM, Nealson KH, Sekiguchi Y, Gorby YA et al. (2012). Functionally stable and phylogenetically diverse microbial enrichments from microbial fuel cells during wastewater treatment. *PLoS One* **7**: e30495.

Ishii S, Suzuki S, Norden-Krichmar TM, Tenney A, Chain PS, Scholz MB et al. (2013). A novel metatranscriptomic approach to identify gene expression dynamics during extracellular electron transfer. *Nat Commun* **4**: 1601.

Jung S, Regan JM. (2011). Influence of external resistance on electrogenesis, methanogenesis, and anode prokaryotic communities in microbial fuel cells. *Appl Environ Microbiol* **77**: 564–571.

Karlin S, Altschul SF. (1990). Methods for assessing the statistical significance of molecular sequence features by using general scoring schemes. *PNAS* **87**: 2264–2268.

Kato S, Hashimoto K, Watanabe K. (2013). Iron-oxide minerals affect extracellular electron-transfer paths of *Geobacter* spp. *Microbes Environ* **28**: 141–148.

Kato S, Nakamura R, Kai F, Watanabe K, Hashimoto K. (2010). Respiratory interactions of soil bacteria with (semi)conductive iron-oxide minerals. *Environ Microbiol* **12**: 3114–3123.

Kiely PD, Regan JM, Logan BE. (2011). The electric picnic: synergistic requirements for exoelectrogenic microbial communities. *Curr Opin Biotechnol* **22**: 378–385.

Luo J, Yang J, He H, Jin T, Zhou L, Wanga M, Zhou M. (2013). A new electrochemically active bacterium phylogenetically related to *Tolumonas osonensis* and power performance in MFCs. *Bioresour Technol* **139**: 141–148.

Logan BE, Hamelers B, Rozendal R, Schroder U, Keller J, Freguia S et al. (2006). Microbial fuel cells: methodology and technology. *Environ Sci Technol* **40**: 5181–5192.

Logan BE. (2008). Chapter 4 Power generation. *Microbial Fuel Cells*. John Wiley & Sons: Hoboken, NJ, USA, pp 44–60.

Lovley DR, Holmes DE, Nevin KP. (2004). Dissimilatory Fe(III) and Mn(IV) reduction. *Adv Microb Physiol* **49**: 219–286.

Lovley DR. (2006). Microbial fuel cells: novel microbial physiologies and engineering approaches. *Curr Opin Biotechnol* **17**: 327–332.

McLean JS, Wanger G, Gorby YA, Wainstein M, McQuaid J, Ishii S et al. (2010). Quantification of electron transfer rates to a solid phase electron acceptor through the stages of biofilm formation from single cells to multicellular communities. *Environ Sci Technol* **44**: 2721–2727.

Nealson KH, Saffarini D. (1994). Iron and manganese in anaerobic respiration: environmental significance, physiology, and regulation. *Annu Rev Microbiol* **48**: 311–343.

Nealson KH. (1997). Sediment bacteria: who's there, what are they doing, and what's new? *Annu Rev Earth Planet Sci* **25**: 403–434.

Nealson KH, Belz A, McKee B. (2002). Breathing metals as a way of life: geobiology in action. *Antonie Van Leeuwenhoek* **81**: 215–222.

Nercessian O, Parot S, Delia ML, Bergel A, Achouak W. (2012). Harvesting electricity with Geobacter bremensis isolated from compost. *PLoS One* **7**: e34216.

Pant D, Van Bogaert G, Diels L, Vanbroekhoven K. (2010). A review of the substrates used in microbial fuel cells (MFCs) for sustainable energy production. *Bioresource Technology* **101**: 1533–1543.

Park HS, Kim BH, Kim HS, Kim HJ, Kim GT, Kim M *et al.* (2001). A novel electrochemically active and Fe(III)-reducing bacterium phylogenetically related to *Clostridium butyricum* isolated from a microbial fuel cell. *Anaerobe* **7**: 297–306.

Pham CA, Jung SJ, Phung NT, Lee J, Chang IS, Kim BH *et al.* (2003). A novel electrochemically active and Fe(III)-reducing bacterium phylogenetically related to *Aeromonas hydrophila*, isolated from a microbial fuel cell. *Fems Microbiol Lett* **223**: 129–134.

Rabaey K, Verstraete W. (2005). Microbial fuel cells: novel biotechnology for energy generation. *Trends Biotechnol* **23**: 291–298.

Sessitsch A, Weilharter A, Gerzabek MH, Kirchmann H, Kandeler E. (2001). Microbial population structures in soil particle size fractions of a long-term fertilizer field experiment. *Appl Environ Microbiol* **67**: 4215–4224.

Shimoyama T, Komukai S, Yamazawa A, Ueno Y, Logan BE, Watanabe K. (2008). Electricity generation from model organic wastewater in a cassette-electrode microbial fuel cell. *Appl Microbiol Biotechnol* **80**: 325–330.

Summers ZM, Fogarty HE, Leang C, Franks AE, Malvankar NS, Lovley DR. (2010). Direct exchange of electrons within aggregates of an evolved syntrophic coculture of anaerobic bacteria. *Science* **330**: 1413–1415.

ter Braak CJF. (1986). Canonical correspondence analysis: a new eigenvector technique for multivariate direct gradient analysis. *Ecology* **67**: 1167–1179.

Thauer RK, Jungermann K, Decker K. (1977). Energy conservation in chemotrophic anaerobic bacteria. *Bacteriol Rev* **41**: 100–180.

Torres CI, Krajmalnik-Brown R, Parameswaran P, Marcus AK, Wanger G, Gorby YA *et al.* (2009). Selecting anode-respiring bacteria based on anode potential: phylogenetic, electrochemical, and microscopic characterization. *Environ Sci Technol* **43**: 9519–9524.

Torsvik V, Ovreas L. (2002). Microbial diversity and function in soil: from genes to ecosystems. *Curr Opin Microbiol* **5**: 240–245.

Tsujimura S, Fujita M, Tatsumi H, Kano K, Ikeda T. (2001). Bioelectrocatalysis-based dihydrogen/dioxygen fuel cell operating at physiological pH. *Physical Chemistry Chemical Physics* **3**: 1331–1335.

Wagner RC, Call DF, Logan BE. (2010). Optimal set anode potentials vary in bioelectrochemical systems. *Environ Sci Technol* **44**: 6036–6041.

Watanabe K, Kodama Y, Harayama S. (2001). Design and evaluation of PCR primers to amplify bacterial 16S ribosomal DNA fragments used for community fingerprinting. *J Microbiol Methods* **44**: 253–262.

Weber KA, Achenbach LA, Coates JD. (2006). Microorganisms pumping iron: anaerobic microbial iron oxidation and reduction. *Nat Rev Microbiol* **4**: 752–764.

White HK, Reimers CE, Cordes EE, Dilly GF, Girguis PR. (2009). Quantitative population dynamics of microbial communities in plankton-fed microbial fuel cells. *ISME J* **3**: 635–646.

Yi H, Nevin KP, Kim B-C, Franks AE, Klimes A, Tender LM *et al.* (2009). Selection of a variant of *Geobacter sulfurreducens* with enhanced capacity for current production in microbial fuel cells. *Biosens Bioelectron* **24**: 3498–3503.

Supplementary Information accompanies this paper on The ISME Journal website (http://www.nature.com/ismej)